Quantitative studies on the microstructures of ternary CaO-Al_2O_3-SiO_2 glasses, melts and correlation with their high-temperature viscosities

Jinglin You[1], Xiaohui Tang[2], Fu Zhang[3], Aurélien Canizarès[4], Catherine Bessada[5], Liming Lu[6], Kai Tang[7], Qingli Zhang[8], Songming Wan[9]

1.Professor, SKLASS, Shanghai University, Shanghai 200444, China. Email: jlyou@staff.shu.edu.cn
2.Doctor, SKLASS, Shanghai University, Shanghai 200444, China
3.Doctor, SKLASS, Shanghai University, Shanghai 200444, China
4.Senior Scientist, CNRS, CEMHTI UPR3079, Université d'Orléans, Orléans, France
5.Professor, CNRS, CEMHTI UPR3079, Université d'Orléans, Orléans, France
6.Senior Scientist, Queensland Centre for Advanced Technologies, Technology Court, CSIRO Mineral Resources, Pullenvale, Queensland, 4069, Australia
7.Senior Scientist, SINTEF AS, 7034 Trondheim, Norway. Email: kai.tang@sintef.no
8.Researcher, Anhui Key Laboratory for Photonic Devices and Materials, Anhui Institute of Optics and Fine Mechanics, Chinese Academy of Sciences, Hefei 230031, China
9.Researcher, Anhui Key Laboratory for Photonic Devices and Materials, Anhui Institute of Optics and Fine Mechanics, Chinese Academy of Sciences, Hefei 230031, China

Keywords: Molten slag, High temperature Raman spectroscopy, NMR, quantum chemistry *ab initio*, Viscosity

ABSTRACT

Microstructure of CaO-SiO_2-based glassy samples with various Al_2O_3 contents were examined quantitatively by Raman spectroscopy and ^{27}Al MAS NMR. Sequence of multiple cluster models of aluminosilicate system modified with Ca^{2+} and Na^{+} cations have been designed, and Raman spectra simulation were carried out after geometric optimization by quantum chemistry (QC) *ab initio* calculation. The functional relationship between Raman scattering cross section (*RSCS*) and stress index of silicon-oxygen tetrahedron (*SIT*) for aluminosilicates was established, which was applied to the calibration of experimental Raman spectra. Some five-fold coordinated aluminum (Al^{V}, around 5%) and less than 2% six-fold coordinated aluminum (Al^{VI}) were detected by ^{27}Al MAS NMR, while most of aluminum remained in tetrahedral sites (Al^{IV}). The hyperfine quantitative results of Raman spectroscopy and NMR showed a gradually production of Al^{IV} with addition of Al_2O_3, along with the significant adjustment of Q_i species distribution, in which Q_1, Q_2 reduced and fully polymerized Q_4 increased while Q_3 showed a non-monotonic variation and obtained the maximum at Al_2O_3=18 mol%. Furthermore, the effects of aluminum to bridging oxygen bond types (T-O_b, T=Si, Al) and the degree of polymerization were also discussed in detail. The evolution of microstructure and its correlation with the viscosity of CaO-SiO_2 based melts, incorporating various Al_2O_3 additives, have been investigated by employing *in situ* high temperature Raman spectroscopy at 1823 K and viscosity model. These structural features related to composition are essential theoretic foundation to understand their properties. The average Q_i evolution culminates in an overall enhancement of the degree of polymerization. Viscosity was determined utilizing a rigorously selected viscosity model, elucidating a consistent upward trajectory as Al_2O_3 content is incrementally added. Furthermore, a quantitative analysis of the relationship between viscosity and structure was conducted based on the average number of non-bridging oxygen per network-forming tetrahedron (NBO/T). It provides valuable insights for examining and predicting viscosity behaviour of aluminosilicate systems.

1. INTRODUCTION

CaO-Al_2O_3-SiO_2 (CAS) glasses and melts are of special interest for their technological significance and structural peculiarities, and have a wide range of industrial applications [Sharma *et al*. (2020), Sokol *et al*. (2018), Li *et al*. (2014)]. For instance, the CAS system is a major component of blast furnace (BF) slags and mold fluxes extensively used in metallurgical processes [Takahashi *et al.* (2015)]. A comprehensive understanding of the physical properties of aluminosilicate molten slags, encompassing thermal conductivity, density, and viscosity, is indispensable for unraveling the intricate mass, momentum, and energy transfer phenomena. This knowledge is crucial for optimizing slag compositions, enhancing fuel usage efficiency, and achieving superior performance in diverse industrial processes [Wang *et al*. (2020), Siafakas *et al*. (2018), Rajavaram *et al*. (2017)]. Among these properties, viscosity hold critical significance in metallurgical melts, in view of its direct effect on the kinetic and thermodynamical conditions of the processes. Therefore, the comprehensive investigation of viscous behavior of molten slags carries imperative theoretical and practical implications for comprehending the fluid dynamic and slag-metal reaction kinetics during the metallurgical processes.

In the ternary CAS system, the network former SiO_2 constructs various structural units through diverse connections of silicon-oxygen tetrahedrons (SiOTs), such as monomer (SiO_4), dimer (Si_2O_7), chain (SiO_3), layered (Si_2O_5) and three-dimensional network structures (SiO_2). These structural units can also be indicated by primary structural species Q_i (i = 0-4, denotes the number of bridging oxygen (BO, O_b) in each tetrahedron) [Sano *et al*. (1997)]. Moreover, You *et al*. (2005) stated that the complex connections among SiOTs cannot be described by primary structure species alone, and hyperfine secondary structures adopted the shorthand symbol $Q^{jklm}_{i\ (n_1h,\ n_2q,\ n_3t)}$ must be adopted, where subscript *i* refers to the number of BO of the central SiOT; superscript *j*, *k*, *l* and *m* correspond to the numbers of BO of the adjacent tetrahedra Q_j, Q_k, Q_l and Q_m of the central Q_i, respectively; n_1, n_2 and n_3 are the number of various rings involved in the central SiOT, respectively, while *h*, *q* and *t* represent six-, four- and three- membered rings, respectively.

Aluminum, as a representative amphoteric oxide, may exhibit different coordination roles, in which the four-fold coordinated AlOT is commonly observed as the network former, facilitating polymerization of the network by consuming alkali metal or alkaline-earth metal cations for charge

compensation. Additionally, the existence of five- and/or six-fold coordinated aluminum has been detected in aluminosilicate, although their definitive structural characteristics and formation mechanisms remain elusive, thereby adding complexity to the overall structure and viscosity behavior [Mysen *et al*. (2021)]. Extensive research has been undertaken to elucidate the amphoteric behavior of Al_2O_3 in aluminosilicate and establish the correlation between structure and viscosity [Zhang *et al*. (2013), Chen *et al*. (2019), Gu *et al*. (2020), Atila *et al*. (2019), Losq *et al*. (2014)]. Park *et al.* (2008) conducted an assessment on the viscosity of CaO-Al_2O_3-SiO_2 slag, revealing an initial increase in viscosity upon the addition of Al_2O_3, followed by a subsequent decrements at higher Al_2O_3 concentrations. However, their analysis of viscous flow behavior was predominantly based on a qualitative examination of the structural aspects. The majority of studies thus far have focused on the impact of the CaO/Al_2O_3 ratio on viscosity [Shao *et al*. (2019), Zhen *et al*. (2014)], leaving the investigation of the effect of Al_2O_3 with a fixed CaO/SiO_2 ratio relatively understudied. Therefore, to clearly get insight into the influence of Al_2O_3 on viscosity, it is essential to quantitatively explore the dependence of viscosity on the structural characteristics of molten slags.

In previous studies, amorphous glasses have been commonly employed as surrogate models for investigating the structural properties of melts, primarily due to the obstacles of high temperature experimental techniques in studying the structural characteristics of molten systems [Chen *et al*. (2019), Viet *et al*. (2016)]. However, numerous investigations have highlighted that the microstructure of silicate and aluminosilicate glasses may not be entirely representative of their corresponding melts, potentially stemming from divergent thermal histories influencing the glass microstructure [Richet *et al*. (2022), Mysen *et al*. (2003)]. The rapid advancement of high-temperature measurement techniques has underscored the pressing need to directly investigate the microstructural characteristics of molten systems. Among them, *in situ* high temperature Raman spectroscopy stands out for its exceptional capability to probe the microstructure of molten substance because of its remarkable sensitivity to the network microstructure, including short-range environment and network connectivity. Some researchers have conducted deep quantitatively analysis of melt structure evolution using *in situ* high temperature Raman spectroscopy in binary CaO-SiO_2, ternary MgO-CaO-SiO_2, and Na_2O-Al_2O_3-SiO_2 system [Mysen *et al*. (2003), Gong *et al*. (2022), Ma *et al*. (2020)]. For ternary CAS system, because of the high melt point and complex amphoteric behavior of Al_2O_3, the information of melt microstructure is absent. As such, it is significant to examine the microstructure of CAS melts by using *in situ* high temperature Raman spectroscopy, and further construct the relationship between structure and properties, which is essential in understanding the fundamental mechanisms of various compositional effect on the macroscopic physical properties.

In the Raman spectra of aluminosilicate, the characteristic Raman-active band in the high wavenumber range (> 800 cm^{-1}) can be assigned to the symmetric stretching vibration of the NBO of SiOT (Si-O_{nb}). This band, is approximately monotonically related to the type of central SiOT, i.e., delicate $Q^{jklm}_{i\ (n_1h,\ n_2q,\ n_3t)}$ or primary Q_i species with different connections between central SiOT and adjacent tetrahedra, and is the object of Raman spectra quantification. Nonetheless, quantitative analysis by Raman spectroscopy is still being developed, You *et al*. (2005) proposed a concept involving the stress index of silicon-oxygen tetrahedra (*SIT*) to reflect the complex connectivities among SiOTs. This was performed to establish a relationship between the Raman scattering cross section (*RSCS*) and *SIT* and further quantitatively analyze the microstructures of binary sodium silicate.

Therefore, in the present work, *SIT* and *RSCS* values were employed to help quantitatively investigate the evolution of delicate $Q^{jklm}_{i\ (n_1h,\ n_2q,\ n_3t)}$ and primary Q_i species by Raman spectroscopy and simulate calcium aluminosilicate glasses and melts that exhibit various Al_2O_3 contents with a fixed CaO/SiO_2 ratio of 1. Additionally, viscosity predictions were carried out through the Urban model, and then to bridge of the correlation between melt microstructure and viscosity.

2. EXPERIMENTAL METHODS

2.1. Material synthesis

Six calcium aluminosilicate glassy samples were prepared by melting mixtures of CaO, Al_2O_3, and SiO_2. The compositions of the samples, ranging from 0 to 30 mole percentage of Al_2O_3 with a constant CaO/SiO_2 ratio of 1, are presented in Table 1. The starting materials with stoichiometric amounts of CaO, Al_2O_3 and SiO_2 (analytical reagent-grade, Sinopharm Chemical Reagent Co., Ltd) were accurately weighed and thoroughly mixed in an agate mortar with ethyl alcohol for 2 h. Subsequently, the mixtures were premelted placed in a muffle furnace at a rate of 10 K/min until 1873 K (above the liquidus temperature of the samples) was reached, and held for 1 h to obtain a homogeneous and bubble-free melt. The resulting liquids were cooled, ground into powder, and then pressed into thin sheets with a diameter of 10 mm and a height of 1 mm. An aerodynamic levitation (ADL) furnace equipped with two beams of CO_2 lasers approximately 80 W and capable of achieving an extremely high cooling rate of 300 K/s was applied to prepare the glassy samples. CASx (x = 0, 6, 12, 18, 24, 30) was adopted as a shorthand notation for the glassy samples with compositions of $(100\text{-}x)/2CaO{\cdot}xAl_2O_3{\cdot}(100\text{-}x)/2SiO_2$.

TABLE 1 – Chemical compositions of calcium aluminosilicate glassy samples

Sample number	CaO/mol%	Al_2O_3/mol%	SiO_2/mol%
CAS0	50	0	50
CAS6	47	6	47
CAS12	44	12	44
CAS18	41	18	41
CAS24	38	24	38
CAS30	35	30	35

2.2. Experimental details

Raman spectra of the vitrified and molten samples were recorded in the range of 50-1600 cm^{-1} by using Horiba Jobin Y'von (LabRam HR) micro-Raman spectrometer equipped with pulse laser with a wavelength of 532 nm and ICCD (Intensified Charge Coupled Device). Six vitrified powders of CASx (x = 0, 6, 12, 18, 24, 30) were placed in a platinum crucible and then heated at a rate of 300 K/min from RT to 1273 K by using a high temperature observational system (IRF-DP, Japan), followed by a subsequent ramp-up from 1273 K to 1823 K at a rate of 100 K/min. After melting, the Raman spectra were recorded at 1823 K.

^{27}Al MAS NMR spectra of glassy samples were collected using a Bruker Advance III WB 400 MHz spectrometer at a Larmor frequency of 104.25 MHz (9.4 T). The samples were spun in cylindrical aluminum free zirconia rotors with a diameter of 4 mm at a spinning rate of 12 kHz. One-pulse acquisition was used while the cycle delay time was 0.5 s, and the cumulative times were 600.

2.3. Computational details

The model clusters of ternary $CaO\text{-}Al_2O_3\text{-}SiO_2$ aluminosilicate with different aluminum introduction and various Q_i connections were constructed on the basis of $CaO\text{-}SiO_2$ binary silicates, which were optimized and calculated by QC *ab initio* calculations by using Gaussian 09W software. The Restricted Hartree-Fock (RHF) self-consistent field and 6-31G(d) basis set were employed to optimize clusters and Raman spectra were then simulated for those clusters after being optimized on the same computational methodology [Nowak *et al*. (1994), Lee *et al*. (1993)].

Notably, the 'Loewenstein Al avoidance' rule [Loewenstein *et al.* (1954)] was preferentially considered for the introduction position and amount of Al of model cluster construction. Considering the charge balance of AlOTs, a cluster structure with n(Al) requires 1/2n(Ca) for charge compensation, which greatly increases the difficulty of cluster structure construction to maintain higher symmetry and reduces computational success. Therefore, the Na^+ cation was selected to

partially displace the Ca^{2+} cation as a charge compensated ion to simulate more reliable structures. Previous studies showed that the influence of different alkali metal and alkaline earth metal cations on the symmetric stretching vibration frequency of Si-O_{nb} in silica tetrahedral structure units can be negligible [Piriou *et al.* (1983), Brawer *et al.* (1977)].

3. RESULTS AND DISCUSSIONS

3.1. Quantification of microstructure of CaO-Al_2O_3-SiO_2 glasses and melts

In this work, a series of model clusters were designed with connections of AlOTs and SiOTs as network formers, Ca^{2+} cations acted as network modifiers, and Na^{+} cations were used, as they are needed to balance the charge of AlOTs. The optimized model clusters by QC *ab initio* calculations with different connections are illustrated in Figure 1. The calculated Raman-active wavenumbers of the symmetric stretching vibrations of Si-O_{nb} and its *RSCS* are shown in Table 2 The calculation results indicate that the characteristic peaks with notable intensity in 800-1200 cm^{-1} are mainly the symmetric stretching vibrations of Si-O_{nb}. The wavenumbers of identical Q_i species in this range decreased with increasing aluminum introduction, which is consistent with the results obtained for kyanite, sillimanite and andalusite by Feng *et al.* (2006). Compared to the Si-O bond, the Al-O bond has a smaller force constant, and the coupling of the Al-O and Si-O bonds leads to a decrease in the wavenumber of the Si-O_{nb} symmetrical stretching vibration.

In order to explain the microscopic stress functioning mechanism and establish the relationship between wavenumbers and microstructures, the *SIT* of SiOT was empirically defined by You. *et al.* (2005). As mentioned above, the introduction of aluminum heavily affects the symmetrical stretching vibration of Si-O_{nb}. Therefore, to establish the relationship between microstructural stress and characteristic Raman vibration wavenumbers in the ternary CaO-Al_2O_3-SiO_2 system, the influence of aluminum on the microscopic stress environment must be considered. The developing calculation formula of *SIT* is as follows:

$$SIT = {}^{1}X_i + \alpha R \tag{1-1}$$

$${}^{1}X_i = \frac{1}{i}\left(\sum_{j=1}^{k} \sqrt{Q_i Q_{(j)}} + \beta \sum_{j=k+1}^{i} \sqrt{Q_i Q_{(j)}} \right) \tag{1-2}$$

$$R = \sum_{1}^{m} \frac{n_{Si} + \beta n_{Al}}{n_i \left(n_i - 2 \right)} \tag{1-3}$$

where ${}^{1}X_i$ is the first-order molecular connectivity index of SiOT, while R and α are the contribution of the ring and proportionality coefficient (α = 1 in nonalumina silicate), respectively. Q_i is the number of BO in the ith SiOT, while Q_j is the BO number of SiOT or AlOT adjacent to the ith SiOT. The parameter n_i is the number of rings Q_i participates in while n_{Si} and n_{Al} are the number of rings SiOT and AlOT participate in, respectively. β is a constant (β = 0.5). The *SIT* values in the clusters are presented in Table 2.

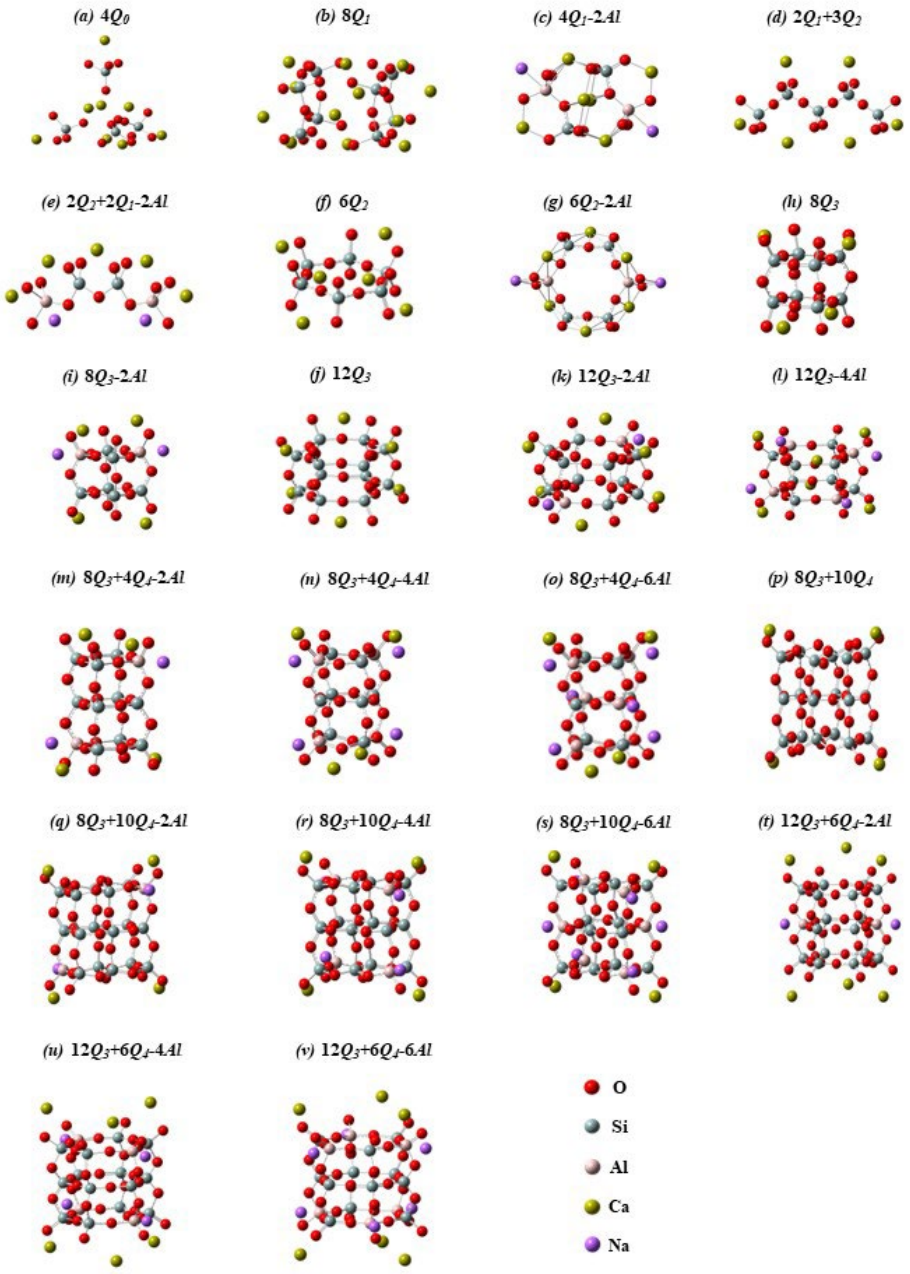

Fig. 1. Diagrams of model clusters with different connections between the central silicon-oxygen tetrahedron (SiOT) and adjacent SiOT or aluminum-oxygen tetrahedra (AlOT), forming a network framework. Additionally, Ca^{2+} cations act as network modifiers, and Na^{+} cations act as charge compensators of AlOTs, partially replacing Ca^{2+} : (a) $Ca_8Si_4O_{16}$; (b) $Ca_{12}Si_8O_{28}$; (c) $Ca_6Na_2Si_2Al_2O_{14}$; (d) $Ca_6Si_5O_{16}$; (e) $Ca_5Si_4O_{13}$; (f) $Ca_6Si_6O_{18}$; (g) $Ca_6Na_2Si_4Al_2O_{18}$; (h) $Ca_4Si_8O_{20}$; (i) $Ca_4Na_2Si_6Al_2O_{20}$; (j) $Ca_6Si_{12}O_{30}$; (k) $Ca_6Na_2Si_{10}Al_2O_{30}$; (l) $Ca_6Na_4Si_8Al_4O_{30}$; (m) $Ca_4Na_2Si_{10}Al_2O_{28}$; (n) $Ca_4Na_4Si_8Al_4O_{28}$; (o) $Ca_4Na_4Si_6Al_6O_{28}$; (p) $Ca_6Na_2Si_{16}Al_2O_{42}$; (q) $Ca_6Na_4Si_{14}Al_4O_{42}$; (r) $Ca_6Na_6Si_{12}Al_6O_{42}$; (s) $Ca_4Si_{18}O_{40}$; (t) $Ca_4Na_2Si_{16}Al_2O_{40}$; (u) $Ca_4Na_4Si_{14}Al_4O_{40}$; (v) $Ca_4Na_4Si_{14}Al_4O_{40}$.

TABLE 2 – The stress index of silicon-oxygen tetrahedron (SIT), Raman scattering cross section (RSCS), and the wavenumber of symmetric stretching vibration of Si-O_{nb} by quantum chemistry *ab initio* calculation of designed model clusters probably existed in ternary CaO-Al_2O_3-SiO_2 glasses and melts.

Chemical formula	Q_i species	*SIT*	*RSCS*	Si-O_{nb} stretching/cm^{-1}
(a) $Ca_8Si_4O_{16}$	$4Q_0$	0.00	11.39	902
(b) $Ca_{12}Si_8O_{28}$	$8Q_1$	1.00	5.87	949
(c) $Ca_6Na_2Si_2Al_2O_{14}$	$4Q_1$	0.50	9.29	936
(d) $Ca_6Si_5O_{16}$	$2Q_1+3Q_2$	1.71	5.46	1013
(e) $Ca_5Na_2Si_2Al_2O_{13}$	$2Q_1+2Q_2$	1.35	7.58	993
(f) $Ca_6Si_6O_{18}$	$6Q_2$	2.25	5.40	1024
(g) $Ca_6Na_2Si_4Al_2O_{18}$	$6Q_2$	1.71	6.20	983
(h) $Ca_4Si_8O_{20}$	$8Q_3$	4.50	3.47	1149
(i) $Ca_4Na_2Si_6Al_2O_{20}$	$8Q_3$	3.83	1.56	1099
(j) $Ca_6Si_{12}O_{30}$	$12Q_3$	4.25	3.29	1142
(k) $Ca_6Na_2Si_{10}Al_2O_{30}$	$12Q_3$	3.85	1.56	1105
(l) $Ca_6Na_4Si_8Al_4O_{30}$	$12Q_3$	3.30	2.15	1068
(m) $Ca_4Na_2Si_{10}Al_2O_{28}$	$8Q_3+4Q_4$	4.22	2.95	1127
(n) $Ca_4Na_4Si_8Al_4O_{28}$	$8Q_3+4Q_4$	3.41	2.71	1071
(o) $Ca_4Na_4Si_6Al_6O_{28}$	$8Q_3+4Q_4$	2.70	4.24	1021
(p) $Ca_6Na_2Si_{16}Al_2O_{42}$	$12Q_3+6Q_4$	4.13	2.34	1147
(q) $Ca_6Na_4Si_{14}Al_4O_{42}$	$12Q_3+6Q_4$	3.80	1.65	1101
(r) $Ca_6Na_6Si_{12}Al_6O_{42}$	$12Q_3+6Q_4$	3.22	2.07	1064
(s) $Ca_4Si_{18}O_{40}$	$8Q_3+10Q_4$	4.81	4.05	1173
(t) $Ca_4Na_2Si_{16}Al_2O_{40}$	$8Q_3+10Q_4$	4.60	3.33	1154
(u) $Ca_4Na_4Si_{14}Al_4O_{40}$	$8Q_3+10Q_4$	4.18	3.01	1131
(v) $Ca_4Na_4Si_{14}Al_4O_{40}$	$8Q_3+10Q_4$	3.48	1.40	1108

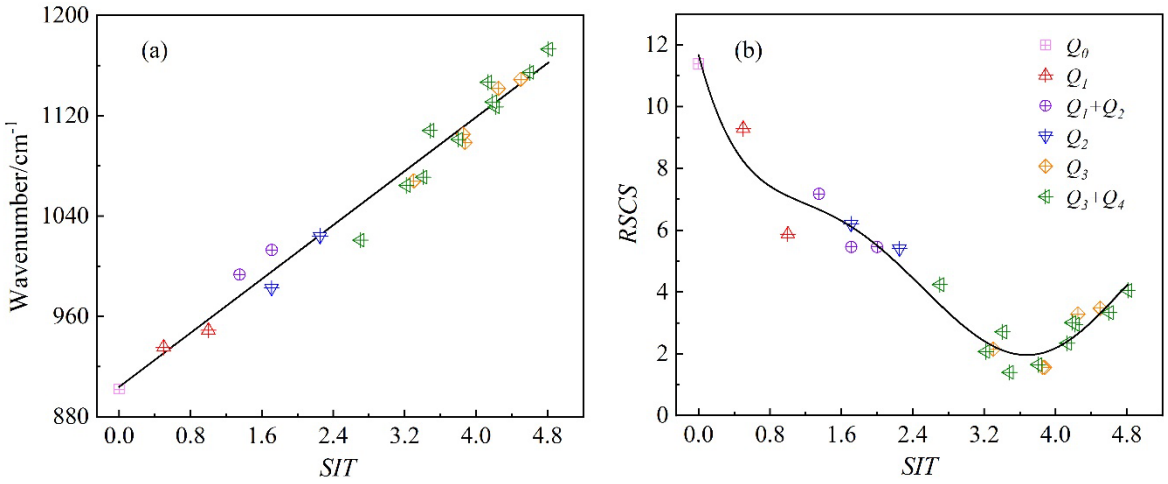

Figure 2. (a) Fitted linear relationship (y(x) = 903.91+53.74x, R^2 = 0.91) between stress index of silicon-oxygen tetrahedron (*SIT*) and Wavenumber of Si-O_{nb} symmetric stretching vibration; (b) Fitted relationship between *SIT* and Raman scattering cross section (*RSCS*) by polynomial regression (y(x) = 11.68-11.00x+10.57x^2-5.11x^3+1.06x^4-0.076x^5, R^2 = 0.9554), in which the icons with different shapes and colors refer to the original fitting data (i.e., the calculated Q_i by quantum chemistry *ab initio* calculation based on the designed probable cluster microstructures in calcium aluminosilicate).

The linear relationship between the *SIT* of Q_i and the calculated wavenumber of the Si-O_{nb} symmetric stretching vibration is established, as shown in Figure 2(a), which is consistent with that of binary sodium silicates and calcium silicate in previous studies [You *et al.* (2005), Ma *et al.* (2020)]. The process used to determine this relationship is well proven, specifically, the concept of *SIT* can be extended to ternary calcium aluminosilicate glasses. On the other hand, Q_i with different *SITs* should have a specific *RSCS* value, and the relationship between *SIT* and *RSCS* is shown in Figure 2(b), which was fitted by polynomial regression. This polynomial function can be applied to correct the experimental Raman spectra of glasses, and then the relative concentrations of Q_i in calcium aluminosilicate glasses can be obtained from the areas of the corrected Raman spectra.

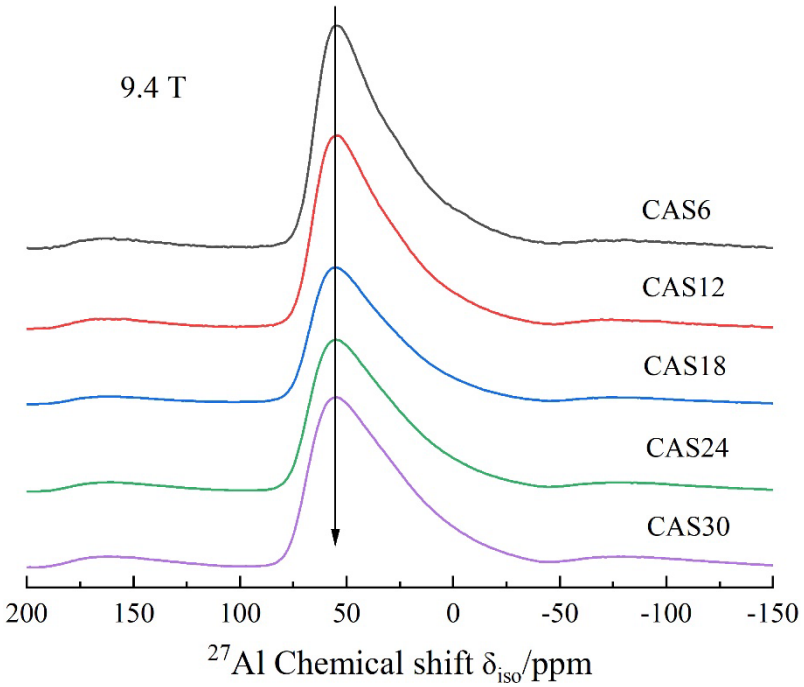

Figure 3. Experimental ^{27}Al MAS NMR spectra of CAS6, CAS12, CAS18, CAS24, and CAS30 glassy samples recorded at a magnetic field of 9.4 T.

3.2. ^{27}Al MAS NMR spectra

^{27}Al MAS NMR spectra can effectively probe subtle variations in the local environment of aluminum. Consequently, to identify the roles of aluminum in the aluminosilicate network, ^{27}Al MAS NMR spectra of the prepared glassy samples were obtained, as shown in Figure 3 The ^{27}Al MAS NMR spectra for the five glasses exhibit a dominant asymmetric peak (approximately 60 ppm) with a shoulder (approximately -20-40 ppm), which denote the chemical shifts of Al^{IV}, Al^{V} and Al^{VI}, respectively. Significantly, the ^{27}Al MAS NMR spectra in this study were recorded at a relatively moderate magnetic field intensity (9.4 T), resulting in a long intensity tail at lower frequency due to the strong second-order quadrupolar coupling effect of aluminum; this occurs because quadrupolar coupling constants (C_Q) are widely distributed at low field strength, which will cover and obscure the possible peaks of Al^{V} and Al^{VI}.

In addition, it can be observed that the NMR spectra show almost an undifferentiated chemical shift and subtle change in full width at half maximum (FWHM). This phenomenon implies that the local environments of aluminum with different constituents did not change significantly, i.e., the presence of aluminum in fourfold coordination predominantly acts as a network former.

To consider the effect of second-order quadrupolar interaction, the spectra were fitted in DMFit [Massiot *et al.* (2002)] software by using Czjzek line shapes, through which the experimental spectra can be fitted with average isotropic chemical shift value (δ_{iso}), distribution, and mean C_Q, to simulate the second-order quadrupolar broadened peaks from aluminum in different coordination environments. The fitting results of the obtained ^{27}Al MAS NMR spectra are shown in Table 3.

TABLE 3 – The fitting parameters of relative intensity (I), average isotropic chemical shift (δ_{iso}), full width at half maximum of the Czjzek distribution (FWHM) and average quadrupolar coupling constant (C_Q) using Czjzek line shapes to the ^{27}Al MAS NMR spectra of glassy samples.

Sample	Coordination environment	I/%	δ_{iso}/ppm	FWHM/ppm	C_Q/MHz
CAS6	Al^{IV}	93.41	65.45	12.86	6.26
	Al^{V}	5.15	33.20	12.76	5.54
	Al^{VI}	1.44	7.97	13.75	5.26
CAS12	Al^{IV}	93.80	66.62	13..36	6.50
	Al^{V}	4.60	35.17	14.39	5.41
	Al^{VI}	1.60	6.57	12.70	5.26
CAS18	Al^{IV}	97.19	67.83	13.89	6.74
	Al^{V}	2.81	34.57	14.39	5.55
	Al^{VI}	-	-	-	-
CAS24	Al^{IV}	96.98	68.76	13.86	7.08
	Al^{V}	3.02	37.84	14.39	5.55
	Al^{VI}	-	-	-	-
CAS30	Al^{IV}	93.11	65.58	12.26	6.33
	Al^{V}	5.25	34.16	14.39	5.73
	Al^{VI}	1.64	7.14	12.70	5.26

For all investigated glasses, most aluminum atoms are in fourfold coordinated Al^{IV} sites (more than 90%, Table 3). Furthermore, a substantial fraction of fivefold coordinated Al^{V} sites are detected (approximately 5%, Table 3) while a minor amount (less than 2%, Table 3) of sixfold coordinated Al^{VI} sites are present. Theoretically, in the peralkaline(-earth) field, aluminum atoms are stabilized in the tetrahedral position without forming higher coordinated species due to having enough Ca^{2+} ions for charge compensation of AlOTs. However, previous studies on ^{27}Al MQ-MAS NMR confirmed that [Stebbins *et al.* (2000), Neuville *et al.* (2007, 2004)], less than 10% of highly coordinated Al^{V} and Al^{VI} were observed even for percalcic CAS glasses. This counterintuitive conclusion is further indicated by the ^{27}Al MAS NMR results for the present samples.

3.3. Raman spectra of calcium aluminosilicate glasses and melts

The glasses and their molten state Raman spectra of all the six samples recorded at 1823K are respectively illustrated in Figure 4 (a) and (b). For the room temperature Raman spectra of glasses, alumina-free CAS0 glass can be roughly distinguished into three regions. For the low-frequency range between 200-400 cm^{-1}, the vibration caused by modifier cations (Ca-O), which can mainly be associated with the lattice vibrations of the skeleton or framework with a broad band centered near 350 cm^{-1}, reflects the long-distance order of the structure. Its relative intensity decreases significantly with the addition of Al_2O_3 until it vanishes completely at x ≥ 18, which indicates that the disorder degree of the silicate network increased violently, and the remaining ordered region of the glassy structure disappeared completely at x ≥ 18. The intermediate frequency range of 400-800 cm^{-1} corresponds to the symmetric bending vibration of the Si-O_b-Si linkages in silicate. For the CAS0 glass, a strong band at 622 cm^{-1} appears, which is assigned to the bending vibrations of Si-O_b-Si linkages. With increasing Al_2O_3 content, the relative intensity decreases sharply and disappears at x > 18. Correspondingly, a new large band grows at 570 cm^{-1} with a shoulder near 508 cm^{-1}, which reflects the motions of bridging oxygen in T-O_b-T linkages (T = Si or Al).

The high-frequency range 800-1200 cm^{-1} is the most informative Raman characteristic band with the strongest relative intensity. Mysen *et al*. (1994) testified that the band in this region belongs to the symmetric stretching vibration of Si-O_{nb}, which is the sum of various Q_i species centered on SiOTs with diverse connections, reflecting the significant microstructural characteristics of aluminosilicates.

Compared with the Raman spectra of glasses, the vibrational bands of Raman spectra of melt exhibit pronounced flattening, along with the broadening of linewidth, due to the introduction of anharmonicity and dynamic disorder resulting from the elevated temperature. Additionally, three major spectral ranges can be distinguished: a low wavenumber range spanning 200-400 cm^{-1} associated with external vibrations involving modifier cations and certain (coupled) deformation modes; an intermediate wavenumber range spanning 400-700 cm^{-1}, indicative of bending vibrations of T-O-T. In the high wavenumber range from 700 to 1200 cm^{-1}, corresponding to the symmetric stretching vibrations of T-O_{nb} bonds, it is noteworthy that the vibrational intensity of Al-O_{nb} within the 700-800 cm^{-1} range can be disregarded due to their significantly lower intensity compared to Si-O_{nb} vibrations.

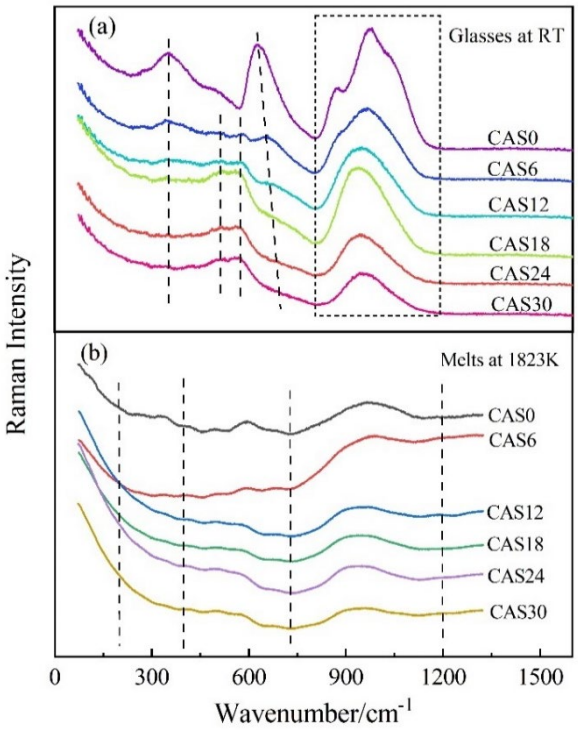

Figure 4. Original Raman spectra of CASx (x = 0, 6, 12, 18, 24, 30): (a) Glasses, and (b) Melts recorded at 1823 K.

3.4. Quantitative analysis of calcium aluminosilicate glasses and melts

Regarding the deconvolution in the high-frequency range (800-1200 cm^{-1}), it should be noted that the original experimental spectra must be calibrated while applying the results of the QC *ab initio* calculation in the experimental quantitative analysis of aluminosilicate microstructure units, including the temperature correction by the Bose-Einstein factor and frequency correction by the excitation sources[You *et al.* (2005), Gong *et al.* (2022), Ma *et al.* (2020)].

As mentioned above, *RSCS* is a significant correction coefficient that concatenates the ratio of Raman peak intensity and the concentration of microstructure species. Therefore, to obtain the microstructure contents of calcium aluminosilicates, Eq. (2) was used to correct the frequency in the original Raman spectra.

$$I(x) = \frac{f(x)}{g(x)} \tag{2}$$

where *I(x)* is the corrected Raman intensity, *f(x)* is the original Raman intensity, and *g(x)* is the functional relationship between the *RSCS* and wavenumber, which was obtained by considering the relationships between wavenumber-*SIT* (Figure 2 (a)) and *RSCS*-*SIT* (Figure 2 (b)) relationships.

Figure 5 (a) and (d) shows the calibration procedure of the original Raman spectra for CASx (x = 0, 6, 12, 18, 24, 30) glass and melt by taking CAS18 sample as a case, in which a significant distinction is uncovered both in shape and peak positions. This is the result of $Q^{jklm}_{i\ (n_1h,\ n_2q,\ n_3t)}$ with different optical sensitivities, and the corrected curve can reflect the authentic $Q^{jklm}_{i\ (n_1h,\ n_2q,\ n_3t)}$ species contents. The delicate structures of glasses and melts are obtained by deconvolution of the corrected Raman spectra, as illustrated by the CAS18 sample in Figure 5 (b) and (e). In addition, the area percentage of Raman bands for Q_i species was determined by summing up all $Q^{jklm}_{i(n_1h,n_2q,n_3t)}$ units with the same BO number i together, and it has been shown in Figure 5 (c) and (f). The area percentage of the calibrated Raman bands assigned to Q_i species from 800 to 1200 cm^{-1} was proportional to the abundance of different Q_i species. In summary, the aforementioned processing techniques for Raman spectra of glasses and melts, encompassing the calibration of original spectra and the meticulous deconvolution of microstructural constituents, facilitate a more rigorous assessment of the distribution of Q_i species within the aluminosilicate system.

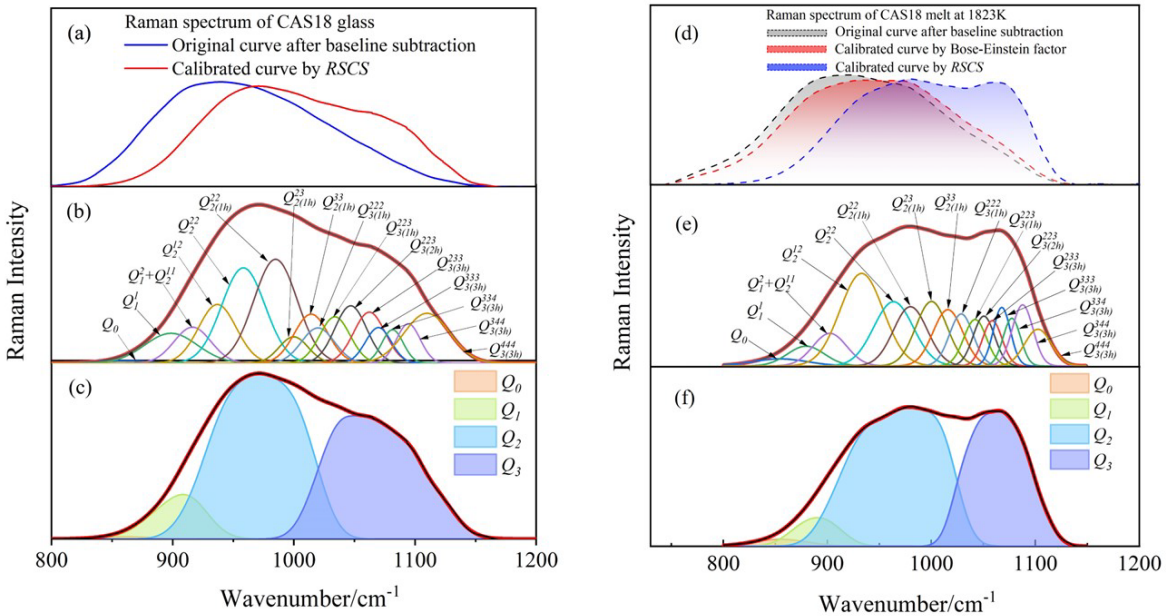

Figure 5. Quantification process of Raman spectra for CAS18 glass (a)-(c) and their corresponding melts (d)-(f). Specifically, (a) and (d): Calibration of the original Raman spectra, (b) and (e): Deconvolution of the calibrated spectrum with delicate $Q^{jklm}_{i(n_1h,n_2q,n_3t)}$ species, (c) and (f): Distribution of primary Q_i species obtained by summing up all the area of delicate $Q^{jklm}_{i(n_1h,n_2q,n_3t)}$ units with the same BO number i.

The quantitative distribution of primary structures Q_i (i = 0, 1, 2, 3, 4) of glasses and melts as a function of Al_2O_3 concentrations is depicted in Figure 6. It shows that the distribution trend of Q_i species in melts is similar to that in glasses, albeit with differences in relative abundances and the continuity of variation. In detail of evolution, both Q_1 and Q_2 decrease with increasing alumina content, while fully polymerized Q_4 exhibits a sustained and drastic augmentation across the entire compositions range. Meanwhile, Q_3 demonstrates a downward convex trend, increasing initially with alumina content up to 12-18 mole%, and decreasing with further alumina additions. Besides, a minimal amount of Q_0 is detected in all vitreous and melting samples. The fluctuation in Q_i distribution, corresponding to varying Al_2O_3 content, attests to the introduction of aluminum, resulting in increased network complexity and connectivity. This outcome is attributed to the preferential consumption of Ca^{2+} ions by AlOTs to achieve charge equilibrium. On the other hand, it displays the richer abundance of Q_2 and Q_4 species in melts than that in glasses, while less Q_3 species was observed in melts. This intriguing phenomenon suggests a potential reaction of $Q_2 + Q_4 \rightarrow Q_3$, taking place during the transformation of the samples from a molten to a vitreous state. It elucidates the propensity for phase separation within the molten state, while the glassification process leans towards the amalgamation of microstructure species.

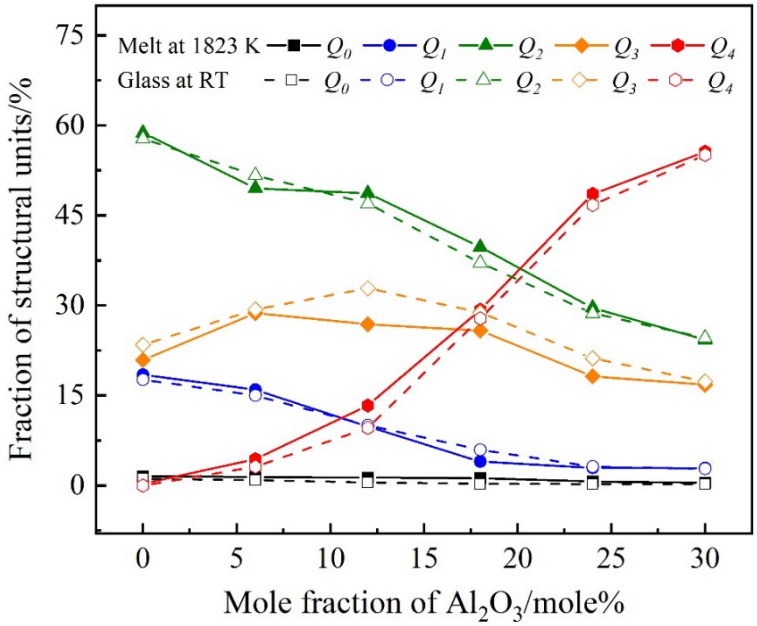

Figure 6. The quantitative distribution of primary Q_i (i = 0-4) species with the increase of Al_2O_3 content determined by Raman spectroscopy in calcium aluminosilicate melts (solid line) and glasses (dashed line).

The distribution of Q_i species in both the glasses and melts highlights a significant convergence in their microstructures, indicating that the melts effectively retain partial microstructure characteristics during the rapid quenching process. Obviously, this is primarily attributed to the utilization of the ADL furnace for sample preparation in this study, which enables the attainment of sufficiently rapid cooling rates. However, it should be emphasized that noticeable disparities in microstructures are anticipated between glasses obtained through slower cooling rates and their corresponding melts. In such cases, conducting *in situ* high temperature Raman spectroscopy directly on the molten state becomes of paramount significance.

3.5. Relationship between microstructural features and viscosity in calcium aluminosilicate melts

In order to obtain reliable viscosity data, the Urbain model was selected for viscosity prediction of CAS samples. The Urbain model, a widely used slag viscosity models in ternary CAS system, relies on WF (Weymann-Frenkel) equation to establish the relationship between compositionally dependent parameters A and B. These parameters are categorized based on the constituents into glass former, modifiers, and amphoterics [Urbain *et al.* (1987, 1982)].

Figure 7 depicts the predicted viscosity values of six calcium aluminosilicate melts at 1823 K by the Urbain model. Meanwhile, six experimental data are given, which have different alumina contents

with fixed ratio CaO/SiO_2 of 1, measured by Zhang *et al.* (2013), Kou *et al.* (1978) and Danek *et al.* (1985) at 1823 K. The graph illustrates a notable agreement between the estimated viscosities and the experimental viscosities, performing a highly consistent trend with increase of alumina. A nearly linear increment is exposed when adding alumina from 0 to 18 mole%, followed by a gradual deceleration in viscosity growth with further increases in alumina content.

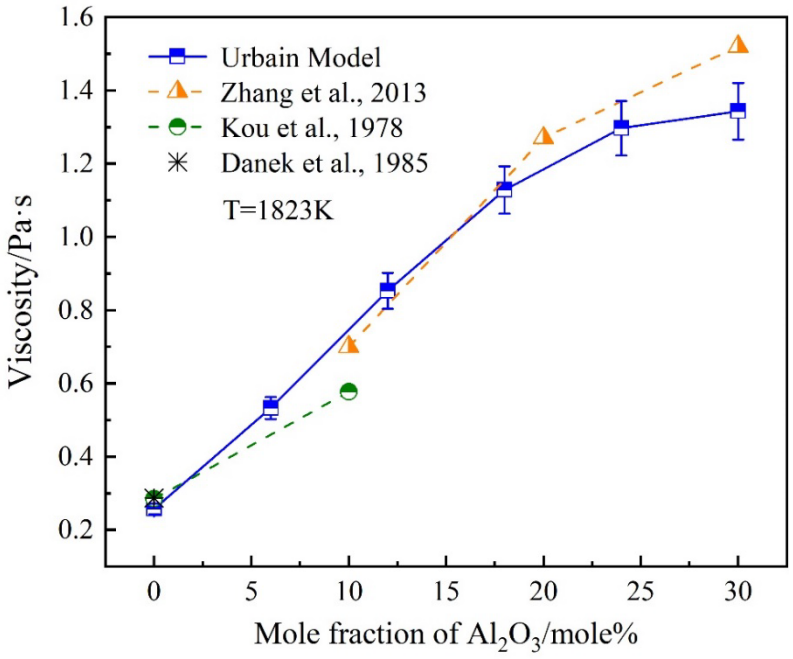

Figure 7. Viscosity values as a function of Al_2O_3 content in calcium aluminosilicate melts at 1823 K. The blue half-solid line presents viscosity values estimated by employing Urbain model, which lacks corresponding experimental viscosity data with the identical composition and temperature. The green and orange dashed dotted line and black icon are experimental values collected from the reference [Zhang *et al.* (2013), Kou *et al.* (1978) and Danek *et al.* (1985)].

In order to gain insight into the viscosity change mechanism, it is significant to correlate the structure evolution with composition variations. Previous studies have manifested that diverse Q_i species exert individual influence on viscosity [Gong *et al.* (2022), Park *et al.* (2013)]. Therefore, it is conceivable to assume that the viscosity variations accompanying the increase in Al_2O_3 content are intricately related to the distribution of Q_i species. As delineated in Figure. 5, for the alumina content is below 12-18 mole%, a monotonic reduction in the concentrations of Q_1 and Q_2 species is observed, concurrent with a continuous ascent in more highly connected species, such as Q_3 and Q_4. This shift in distribution precipitates a linear escalation in viscosity. Conversely, upon exceeding the 12-18 mole% for alumina content, Q_3 begins to diminish, while the monotonic trends of Q_1, Q_2, and Q_4 remain unabated. Moreover, it's noteworthy that when x ≥ 18 mole%, the alumina avoidance parameter (AAP) exceeds 1, signifying the emergence of weaker Al^{IV}-O_b-Al^{IV} bond, which supplants Si-Q_b bonds [Zhang *et al.* (2013)]. These two interplaying factors collectively contribute to a gradual deceleration in the increase of viscosity.

To further ascertain the structural effects on viscosity and establish the quantitative correlation between them, the degree of polymerization (DOP) of network was evaluated which has been borne out a higher DOP tended to induce a higher viscosity in silicate. The DOP is typically quantified by assessing the average number of NBO per coordinated network-forming atom, denoted as NBO/T (T represents the total number of SiOT and AlOT units in the aluminosilicate system). In detail, the value of NBO/T can be obtained by Eq. 3.

$$NBO/T = \frac{n_{SiO_2}\sum_{i=0}^{4}(4-i)X_{Q_i}}{n_{SiO_2}+2n_{Al_2O_3}X_{Al^{IV}}} \quad (3)$$

Figure 8 shows the calculation results of NBO/T of melts by using Raman deconvolution results, as a function of alumina content. For contrastive analysis, the values of NBO/T of glasses is presented in Figure 8. As anticipated, both NBO/T types exhibit a gradual decline with the addition of alumina, evidencing a strengthening of network connectivity. Notably, even though the Q_i distribution between the glass and corresponding melt exhibits noticeable disparities, the DOP between the two remains virtually identical, with no discernible differences. This can be attributed to the collective effect of various Q_i species.

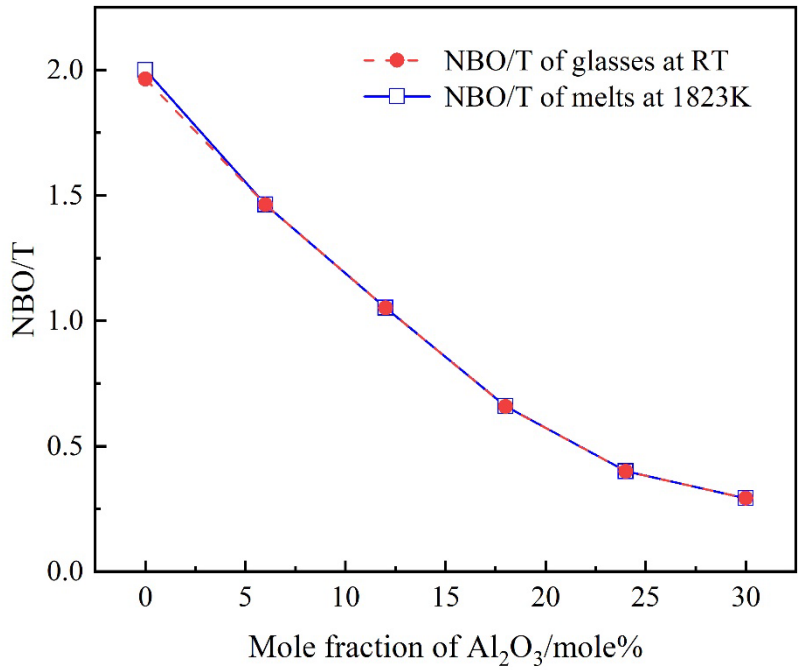

Figure 8. The variation of NBO/T of melts and glasses with adding of alumina.

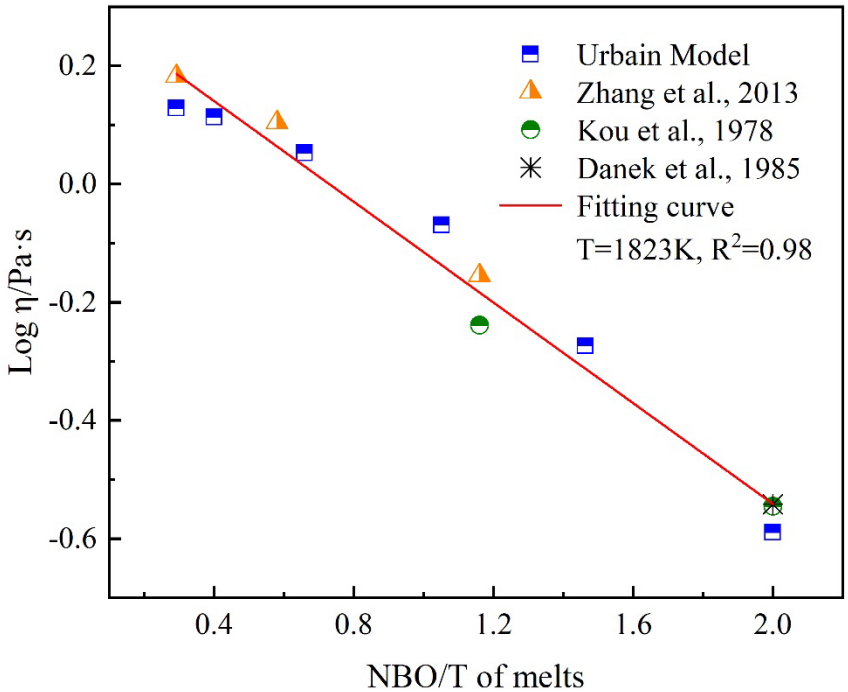

Figure 9. The quantitative linear relationship between the logarithm of viscosities and NBO/T of melts. The blue icon presents viscosity values obtained by Urbain model at 1823 K and red line is the corresponding fitting curve with the function of $\log\eta(Pa\cdot s) = -0.43(NBO/T) + 0.31$

Figure 9 shows the linear fitting results of the logarithm of viscosity and NBO/T of melts at 1823 K. As can be seen, with increasing NBO/T which means that the DOP of melts decreases, the logarithm

of viscosity progressively decreases, which is in accordance with the above analyses. The negative functional relationship between them can be expressed mathematically as Eq. 4:

$$\log\eta(Pa\cdot s) = -0.43\left(NBO/T\right) + 0.31 \quad (4)$$

With the coefficient of determination R^2 of 0.98. In previous studies, Wu *et al.* (2015) established a robust correlation between the logarithm of viscosity and NBO/T of $CaO\text{-}SiO_2$ system by Molecular dynamics simulation method. But for $CaO\text{-}Al_2O_3$ system, the fitting result was deemed inadequate due to the amphoteric nature of alumina, resulting in the more complicated structure. In our present work, an overall remarkable linear correlation is exhibited between the logarithm of viscosity and the experimentally determined NBO/T of melts, which clearly demonstrates the quantitative relationship of them.

4. CONCLUSIONS

The microstructure characteristics and viscosity behavior of $CaO\text{-}SiO_2$-based melts at 1823 K were investigated by incorporating varying Al_2O_3 contents from 0 to 30 mole%. By considering the influence of aluminum, alongside calibrations for temperature and *RSCS*, a refined deconvolution of Raman spectra for CAS glasses and melts have been achieved. Comparative analysis reveals a congruence in Q_i distribution trends between rapidly quenched glass and corresponding melts, implying that a higher cooling rate during glass formation may effectively conserve the in situ structural characteristics of the melts, and the evolution of Q_i conveyed a monotonic augmentation in the DOP across the entire compositional range. Yet, notable discrepancies are also observed, especially for Q_2, Q_3, and Q_4 species, with a potential $Q_2 + Q_4 \rightarrow Q_3$ reaction seems to transpire during the shift from a molten to a vitreous state.

Further exploration of the relationship between composition, microstructure, and viscosity was conducted within the defined compositional range of CAS melts. The results revealed a gradual increase in viscosity with the addition of alumina, displaying a progressively leveling off nonlinear trend. However, a robust linear relationship was observed between the logarithm of viscosity and the DOP quantified by NBO/T.

ACKNOWLEDGMENTS

This work was supported by National Natural Science Foundation of China (21773152), National 111 project (D17002, the Program of Introducing Talents of Discipline to Universities), the Key Basic Research Projects of the Basic Strengthening Plan of the Commission of Science and Technology(2021-JCJQ-ZD-051-00-02), the Shanghai Committee of Science and Technology Fund, China (12520709200), the Open Project Program of the State Key Laboratory of Advanced Special Steel, Shanghai University, China (SKLASS2020-06) and Special Fund Project of Shanghai Municipality for Science and Technology Development (YDZX20173100001316), the China Scholarship Council under the Grant CSC No. 202006890136.

REFERENCES

A. Atila, E.M. Ghardi, A. Hasnaoui, S. Ouaskit, Alumina effect on the structure and properties of calcium aluminosilicate in the percalcic region: A molecular dynamics investigation, Journal of Non-Crystalline Solids, 525 (2019).

S.A. Brawer, W.B. White, Raman spectroscopic investigation of the structure of silicate glasses (II). Soda-alkaline earth-alumina ternary and quaternary glasses, Journal of Non-Crystalline Solids, 23 (1977) 261-278.

Z. Chen, H. Wang, Y. Sun, L. Liu, X. Wang, Insight into the Relationship Between Viscosity and Structure of $CaO\text{-}SiO_2\text{-}MgO\text{-}Al_2O_3$ Molten Slags, Metallurgical and Materials Transactions B, 50 (2019) 2930-2941.

V. Danek, T. Licko, Z. Panek, Viscosity of melts in the system $CaO\text{-}FeO\text{-}Fe_2O_3\text{-}SiO_2$, Silikaty, 29 (1985) 291-299.

P. Feng, Y. Xuehui, M. Xuanxue, Y. Jinglin, W. Chen, C. Hui, J. Guochang, Raman Active Vibrations of Aluminosilicates, Spectroscopy and Spectral Analysis, 26 (2006) 1871-1875.

S. Gu, G. Wen, J. Guo, Z. Wang, P. Tang, Z. Hou, Effect of Al_2O_3 on non-Newtonian property and its relation to structure of mold fluxes during shear stress field at 1573 K, Journal of Non-Crystalline Solids, 547 (2020).

X. Gong, J. Wang, J. You, M. Wang, X. Tang, F. Zhang, K. Tang, L. Lu, S. Wan, Q. Zhang, Room temperature Raman spectroscopy and ^{29}Si MAS NMR combined with high temperature Raman spectroscopy and DFT calculation of $xMgO\text{-}(1\text{-}x)CaO\text{-}SiO_2$ glasses and melts, Ceramics International, 48 (2022) 4911-4920.

T. Kou, K. Mizoguchi, Y. Suginohara, The Effect of Al_2O_3 on the Viscosity of Silicate Melt, Journal of the Japan Institute of Metals and Materials, 42 (1978) 775-781.

C. Le Losq, D.R. Neuville, P. Florian, G.S. Henderson, D. Massiot, The role of Al^{3+} on rheology and structural changes in sodium silicate and aluminosilicate glasses and melts, Geochimica et Cosmochimica Acta, 126 (2014) 495-517.

T.J. Lee, D. Jayatilaka, An open-shell restricted Hartree-Fock perturbation theory based on symmetric spin orbitals, Chemical physics letters, 201 (1993) 1-10.

J.L. Li, Q.F. Shu, K. Chou, Effect of Al_2O_3/SiO_2 mass ratio on viscosity of $CaO-Al_2O_3-SiO_2-CaF_2$ slag, Ironmaking & Steelmaking, 42 (2014) 154-160.

W. Loewenstein, The distribution of aluminum in the tetrahedra of silicates and aluminates, American Mineralogist: Journal of Earth and Planetary Materials, 39 (1954) 92-96.

J. Ma, M. Wang, J. You, K. Tang, L. Lu, S. Wan, J. Wang, X. Gong, Y. Wang, Quantitative studies on the structure of $xCaO\cdot(1-x)SiO_2$ glasses and melts by *in-situ* Raman spectroscopy, ^{29}Si MAS NMR and quantum chemistry *ab initio* calculation, Journal of Non-Crystalline Solids, 546 (2020).

D. Massiot, F. Fayon, M. Capron, I. King, S. Le Calvé, B. Alonso, J.-O. Durand, B. Bujoli, Z. Gan, G. Hoatson, Modelling one- and two-dimensional solid-state NMR spectra, Magnetic Resonance in Chemistry, 40 (2002) 70-76.

B. Mysen, Structure of Aluminosilicate Melts, ISIJ International, 61 (2021) 2866-2881.

B.O. MYSEN, A. LUCIER, G.D. CODY, The structural behavior of Al^{3+} in the system $Na_2O-Al_2O_3-SiO_2$ in peralkaline melts and glasses American Mineralogist, 88 (2003) 1668-1678.

B. Mysen, D. Virgo, Structure and Properties of Silicate Glasses and Melts; Theories and Experiment, Advanced Mineralogy, Springer1994, pp. 238-254.

D.R. Neuville, L. Cormier, D. Massiot, Al environment in tectosilicate and peraluminous glasses: A ^{27}Al MQ-MAS NMR, Raman, and XANES investigation, Geochimica et Cosmochimica Acta, 68 (2004) 5071-5079.

D. Neuville, L. Cormier, V. Montouillout, D. Massiot, Local Al site distribution in aluminosilicate glasses by ^{27}Al MQMAS NMR, Journal of Non-Crystalline Solids, 353 (2007) 180-184.

M. Nowak, H. Rostkowska, L. Lapinski, J. Kwiatkowski, J. Leszczynski, Experimental matrix isolation and theoretical ab initio HF/6-31G (d, p) studies of infrared spectra of purine, adenine and 2-chloroadenine, Spectrochimica Acta Part A: Molecular Spectroscopy, 50 (1994) 1081-1094.

J.H. Park, Structure-Property Relationship of $CaO-MgO-SiO_2$ Slag: Quantitative Analysis of Raman Spectra, Metallurgical and Materials Transactions B, 44 (2013) 938-947.

J.H. Park, H. Kim, D.J. Min, Novel Approach to Link between Viscosity and Structure of Silicate Melts via Darken's Excess Stability Function: Focus on the Amphoteric Behavior of Alumina, Metallurgical and Materials Transactions B, 39 (2008) 150-153.

B. Piriou, P. McMillan, The high-frequency vibrational spectra of vitreous and crystalline orthosilicates, American Mineralogist, 68 (1983) 426-443.

R. Rajavaram, H. Kim, C.-H. Lee, W.-S. Cho, C.-H. Lee, J. Lee, Effect of Al_2O_3 Concentration on Density and Structure of $(CaO-SiO_2)-xAl_2O_3$ Slag, Metallurgical and Materials Transactions B, 48 (2017) 1595-1601.

P. Richet, A. Polian, D. Vo-Thanh, Y. Bottinga, Brillouin scattering in aluminosilicate glasses and melts up to 2550 K. Temperature and composition effects, Journal of Non-Crystalline Solids: X, 14 (2022).

N. Sano, W.-K. Lu, P.V. Riboud, M. Maeda, Advanced physical chemistry for process metallurgy, Academic Press1997.

H. Shao, E. Gao, W. Wang, L. Zhang, Effect of fluorine and CaO/Al_2O_3 mass ratio on the viscosity and structure of $CaO-Al_2O_3$-based mold fluxes, Journal of the American Ceramic Society, 102 (2019) 4440-4449.

L. Sharma, R. Chhibber, Design & development of SAW fluxes using $CaO-SiO_2-CaF_2$ and $CaO-SiO_2-Al_2O_3$ flux systems, Ceramics International, 46 (2020) 1419-1432.

D. Siafakas, T. Matsushita, A.E.W. Jarfors, S. Hakamada, M. Watanabe, Viscosity of $SiO_2-CaO-Al_2O_3$ Slag with Low Silica - Influence of CaO/Al_2O_3, SiO_2/Al_2O_3 Ratio, ISIJ International, 58 (2018) 2180-2185.

V.E. Sokol'skii, D. Pruttskov, V. Busko, V. Kazimirov, O. Roik, A. Chyrkin, V. Galinich, I. Goncharov, Investigation of structure of $CaO-Al_2O_3-SiO_2$ melts as a basis for the development of new agglomerated welding fluxes and industrial refractories, Journal of Mining and Metallurgy, Section B: Metallurgy, 54 (2018) 133-141.

J.F. Stebbins, S. Kroeker, S.K. Lee, T. Kiczenski, Quantification of five-and six-coordinated aluminum ions in aluminosilicate and fluoride-containing glasses by high-field, high-resolution ^{27}Al NMR, Journal of Non-Crystalline Solids, 275 (2000) 1-6.

S. Takahashi, D.R. Neuville, H. Takebe, Thermal properties, density and structure of percalcic and peraluminus $CaO-Al_2O_3-SiO_2$ glasses, Journal of Non-Crystalline Solids, 411 (2015) 5-12.

G. Urbain, Viscosity estimation of slags, Steel research, 58 (1987) 111-116.

G. Urbain, Y. Bottinga, P. Richet, Viscosity of liquid silica, silicates and alumino-silicates, Geochimica et Cosmochimica Acta, 46 (1982) 1061-1072.

U. Veit, C. Rüssel, Y. Houet, D. Laurent, Viscosity and Liquidus Temperature of Ternary Glasses Close to the Eutectic Composition in the $CaO-Al_2O_3-SiO_2$ System, International Journal of Applied Glass Science, 7 (2016) 295-309.

Z. Wang, S. Huang, G. Wen, W. Jiang, F. Chen, P. Tang, Effects of temperature on the thermal conductivity of amorphous $CaO-SiO_2-Al_2O_3$ slags: a computational insight, Phys Chem Chem Phys, 22 (2020) 8808-8816.

T. Wu, S. He, Y. Liang, Q. Wang, Molecular dynamics simulation of the structure and properties for the $CaO-SiO_2$ and $CaO-Al_2O_3$ systems, Journal of Non-Crystalline Solids, 411 (2015) 145-151.

J.L. You, G.C. Jiang, H.Y. Hou, H. Chen, Y.Q. Wu, K.D. Xu, Quantum chemistry study on superstructure and Raman spectra of binary sodium silicates, Journal of Raman Spectroscopy: An International Journal for Original Work in all Aspects of Raman Spectroscopy, Including Higher Order Processes, and also Brillouin and Rayleigh Scattering, 36 (2005) 237-249.

G.-H. Zhang, K.-C. Chou, Influence of Al_2O_3/SiO_2 Ratio on Viscosities of $CaO-Al_2O_3-SiO_2$ Melt, ISIJ International, 53 (2013) 177-180.

Y.-L. Zhen, G.-H. Zhang, X.-L. Tang, K.-C. Chou, Influences of Al_2O_3/CaO and Na_2O/CaO Ratios on Viscosities of $CaO-Al_2O_3-SiO_2-Na_2O$ Melts, Metallurgical and Materials Transactions B, 45 (2014) 123-130.